minerals

MDPI

Article

Hydrogen Effect on the Sound Velocities of Upper Mantle Omphacite

Wade Mans [1,2,*], Jin S. Zhang [1,2,*], Ming Hao [1,2], Joseph R. Smyth [3], Dongzhou Zhang [4,5], Gregory J. Finkelstein [5,6] and Przemyslaw Dera [5]

1 Department of Earth and Planetary Sciences, University of New Mexico, Albuquerque, NM 87131, USA; minghao@unm.edu
2 Institute of Meteoritics, University of New Mexico, Albuquerque, NM 87131, USA
3 Department of Geological Sciences, University of Colorado, Boulder, CO 80309, USA; smyth@colorado.edu
4 GeoSoilEnviroCARS, University of Chicago, Argonne National Laboratory, Argonne, IL 60439, USA; dzhang@hawaii.edu
5 Hawaii Institute of Geophysics and Planetology, University of Hawaii at Manoa, Honolulu, HI 96822 USA; gjfinkel@princeton.edu (G.J.F.); pdera@hawaii.edu (P.D.)
6 Department of Geosciences, Princeton University, Princeton, NJ 08544, USA
* Correspondence: wmans@unm.edu (W.M.); jinzhang@unm.edu (J.S.Z.)

Received: 7 October 2019; Accepted: 6 November 2019; Published: 8 November 2019

Abstract: Clinopyroxene (Cpx) is commonly believed to be the best structural water (hydrogen) carrier among all major upper mantle nominally anhydrous minerals (NAMs). In this study, we have measured the single-crystal elastic properties of a Cpx, a natural omphacite with ~710 ppm water at ambient pressure (P) and temperature (T) conditions. Utilizing the single-crystal X-ray diffraction (XRD) and electron microprobe data, the unit cell parameters and density were determined as a = 9.603(9) Å, b = 8.774(3) Å, c = 5.250(2) Å, β = 106.76(5)°, V = 255.1(4) Å^3, and ϱ = 3.340(6) g/cm^3. We performed Brillouin spectroscopy experiments on four single crystals along a total of 52 different crystallographic directions. The best-fit single-crystal elastic moduli (C_{ij}s), bulk and shear moduli were determined as: C_{11} = 245(1) GPa, C_{22} = 210(2) GPa, C_{33} = 249.6(9) GPa, C_{44} = 75.7(9) GPa, C_{55} = 71.2(5) GPa, C_{66} = 76(1) GPa, C_{12} = 85(2) GPa, C_{13} = 70(1) GPa, C_{23} = 66(2) GPa, C_{15} = 8.0(6) GPa, C_{25} = 6(1) GPa, C_{35} = 34.7(6) GPa, and C_{46} = 8.7(7) GPa, K_{S0} = 125(3) GPa, and G_0 = 75(2) GPa, respectively. Compared with the anticipated elastic properties of an anhydrous omphacite with the same chemical composition, our results indicate that the incorporation of ~710 ppm structural water has no resolvable effect on the aggregate elastic properties of omphacite, although small differences (up to ~9 GPa) were observed in C_{13}, C_{25}, C_{44}, and C_{66}.

Keywords: elasticity; omphacite; clinopyroxene; eclogite; structural water; nominally hydrous minerals; seismic velocities

1. Introduction

Quantifying the water content in the Earth's upper mantle through seismic observations requires the knowledge of how structural water content affects the elastic properties for various nominally anhydrous minerals (NAMs) [1,2]. Whether the upper mantle is universally or locally hydrated is still controversial [3,4], although the water carried down by the subducting slabs is considered a major source of the water in the Earth's interior [5–8]. Subduction is one of the main driving forces of the mantle convection and is responsible for many geological processes in the Earth's interior [9,10]. The basaltic slab crust transforms into eclogite at depths greater than ~100 km and it remains denser than the ambient mantle down to ~600 km depths [11]. As the solid solution between diopside (Di,

$CaMgSi_2O_6$) and jadeite (Jd, $NaAlSi_2O_6$), omphacite is the major mineral phase that constitutes up to 80 vol% of eclogite. The subducting slabs carry the surface water into the Earth's interior primarily in the form of structural water; thus, it is important to know how much structural water can be stored in the major mineral phases in the subducting slabs. The maximum solubility of H_2O—depending on temperature (T) and pressure (P)—in pure Di ranges from 121–568 ppm, but in aluminous Di, this value increases up to 2500 ppm [12]. Natural Clinopyroxene (Cpx) samples can host as high as 2000 ppm water in their crystal structures [12,13], much higher than all other major upper mantle minerals such as olivine, orthopyroxene, or garnet. As a type of Cpx, which can retain the highest amount of water in its structure among all upper mantle NAMs, omphacite is likely both an important water carrier as well as a potential water reservoir in the Earth's interior [5,6,14–17].

Structural water (hydrogen) is incorporated into the Cpx crystal structure through cation vacancies primarily on the M2 site [13,18]. Previous experimental studies on olivine, another NAM commonly found in the ambient upper mantle, have suggested that the incorporation of hydrogen into the NAMs decreases both the *P*-wave and *S*-wave velocities (V_p and V_s) [19–23]. This softening effect of structural water can potentially affect our understanding of the upper mantle seismic structures and mineralogical composition, as well as the total water budget of the Earth's interior [6,21–25]. In addition, there is a growing interest in the mineral physics and petrology communities in using various minerals' thermoelastic parameters to establish new elastic geobarometers for interpreting various deep geological processes that happened in the past [26,27]. Unfortunately, most previous investigations are restricted to hydrous olivine and its high-*P* polymorphs [21–23,28–30], and no experimental sound velocity measurements have previously been made for hydrous Cpx. Therefore, in this study, we performed single-crystal Brillouin spectroscopy experiments on a hydrous omphacite sample with ~710 ppm water in order to study the possible structural water effect on the single-crystal elastic properties of omphacite.

2. Materials and Methods

The omphacite crystals were hand-selected from the natural omphacite sample SBB-46 from the South African Bobbejaan mine. Four different crystals were double-side polished to less than 30 μm thickness. Under optical examination, all crystals were inclusion- and scratch-free. The chemical composition $(Na_{0.396}K_{.005})(Mg_{0.537}Ca_{0.550}Fe_{0.072}Cr_{0.022}Ti_{0.007}Mn_{0.001})Al_{0.433}Si_{1.971}O_6$ (simplified to $Di_{59.1}Jd_{40.9}$) and the ~710 ppm hydrogen content of SBB-46 was determined in [13].

In order to determine the unit cell parameters and crystal orientation, we carried out the single-crystal XRD experiments for the 2 crystals *a* and *b* at ambient *P*–*T* condition at experimental station 13-BM-C, GeoSoilEnviroCARS (GSECARS), Advanced Photon Source, Argonne National Laboratory. The remaining 2 crystals *c* and *d* were measured at ambient *P*–*T* condition in the X-Ray Atlas Diffraction Lab at the University of Hawai'i at Manoa.

At GSECARS, the X-ray beam was monochromated to 28.6 keV with the beam size of ~12 μm × 18 μm determined at the full width at half maximum. The omphacite crystal was placed in an empty DAC, which had an opening angle of ±38°. Two separate detector positions were used by rotating a MAR165 Charge Coupled Device detector on a rotational arm [31]. The first detector angle was perpendicular to the incident X-Ray beam, while the second detector position was offset from the first position by 20° around the horizontal axis. Sample-to-detector distance and detector tilting were calibrated in the Dioptas program [32] using NIST standard LaB_6 powder. The diffraction images were collected in both wide-angle images that covered the whole ±38° opening angle range and 1° step-segments with 1 s/° exposure time. At the X-Ray Atlas Diffraction Lab in University of Hawai'i, a Bruker D8 Venture XRD diffractometer with Incoatec IμS 3.0 AgKα microfocus source, Helios focusing optics, Photon II detector was used for collecting the single-crystal diffraction images at a wide range of scattering angles. Diffraction data from both experiments was processed using Bruker APEX III software. For the needs of this study, full structure refinement was not performed, and only unit cell parameters were refined.

We performed the Brillouin spectroscopy experiments on all 4 double-polished SBB-46 omphacite single crystals at the High-*P* Laser Spectroscopy Laboratory at University of New Mexico. The light source was a 532-nm 300-mW single-mode diode-pumped solid-state laser. The experiment utilized a 50° symmetric forward scattering geometry, with the scattering angle precisely calibrated to be 50.42(5)° using the Corning 7980 standard silica glass [33,34]. V_p and V_s were determined for all 4 pre-oriented samples at ambient *P*–*T* condition for a total of 52 crystallographic directions. Each sample was measured at 13 different χ angles (0°, 30°, 60°, 120°, 150°, 180°, 195°, 225°, 255°, 285°, 315°, 345° and 360°) along the 360° azimuth to account for any possible geometric errors with an average collection time of 10 min per spectrum. The resulting Brillouin spectra all have very high signal-to-noise ratios (Figure 1).

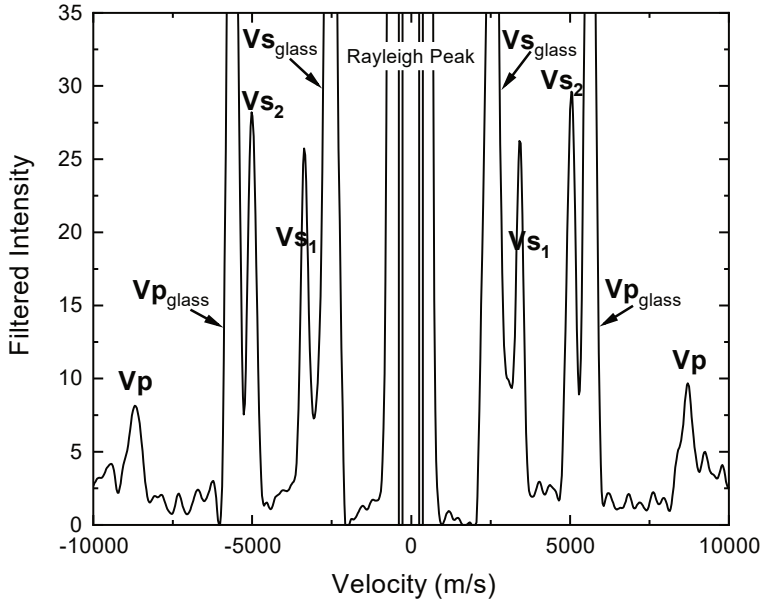

Figure 1. Typical Brillouin spectrum of omphacite crystal *d* at $\chi = 0°$.

3. Results and Discussion

The single-crystal XRD measurements for all four crystals yielded the averaged unit cell parameters of the SBB-46 omphacite of a = 9.603(9) Å, b = 8.774(3) Å, c = 5.250(2) Å, β = 106.76(5)°, V = 255.1(4) cm^3. The planes normal of the four crystals were determined to be: (0.9131 −0.4076 0.0018) for crystal *a*, (−0.2742 0.9457 −0.1748) for crystal *b*, (0.4646 0.1359 −0.8750) for crystal *c*, and (−0.6860 −0.5145 0.5145) for crystal *d* (Figure 2). The density at ambient condition was then calculated as ϱ_0 = 3.340(6) g/cm^3. Omphacite crystals are known to assume one of two different symmetries, depending on the crystallization conditions: the disordered high-temperature phase crystallizes with space group C2/c, whereas the cation-ordered phase crystallizes with space group P2/n [35]. At ambient pressure, the order–disorder transition takes place at 725 °C [36]. The omphacite SBB-46 had a C2/c symmetry based on its high *T* thermal history. The difference in cation ordering was not found to have a resolvable effect on the elastic properties beyond experimental uncertainties [37].

The single-crystal C_{ij}s for the SBB-46 hydrous omphacite under ambient conditions were calculated through the least-squares inversion using the Christoffel equation. The best-fit C_{ij} model was: C_{11} = 245(1) GPa, C_{22} = 210(2) GPa, C_{33} = 249.6(9) GPa, C_{44} = 75.7(9) GPa, C_{55} = 71.2(5) GPa, C_{66} = 76(1) GPa, C_{12} = 85(2) GPa, C_{13} = 70(1) GPa, C_{23} = 66(2) GPa, C_{15} = 8.0(6) GPa, C_{25} = 6(1) GPa, C_{35} = 34.7(6) GPa, and C_{46} = 8.7(7) GPa. The root-mean-square residual was less than 53 m/s between the modeled and observed velocities (Figure 2). The K_{S0} and G_0 were calculated as 125(3) and 75(2) GPa from the single-crystal C_{ij}s under the Voigt-Reuss-Hill averaging scheme [38].

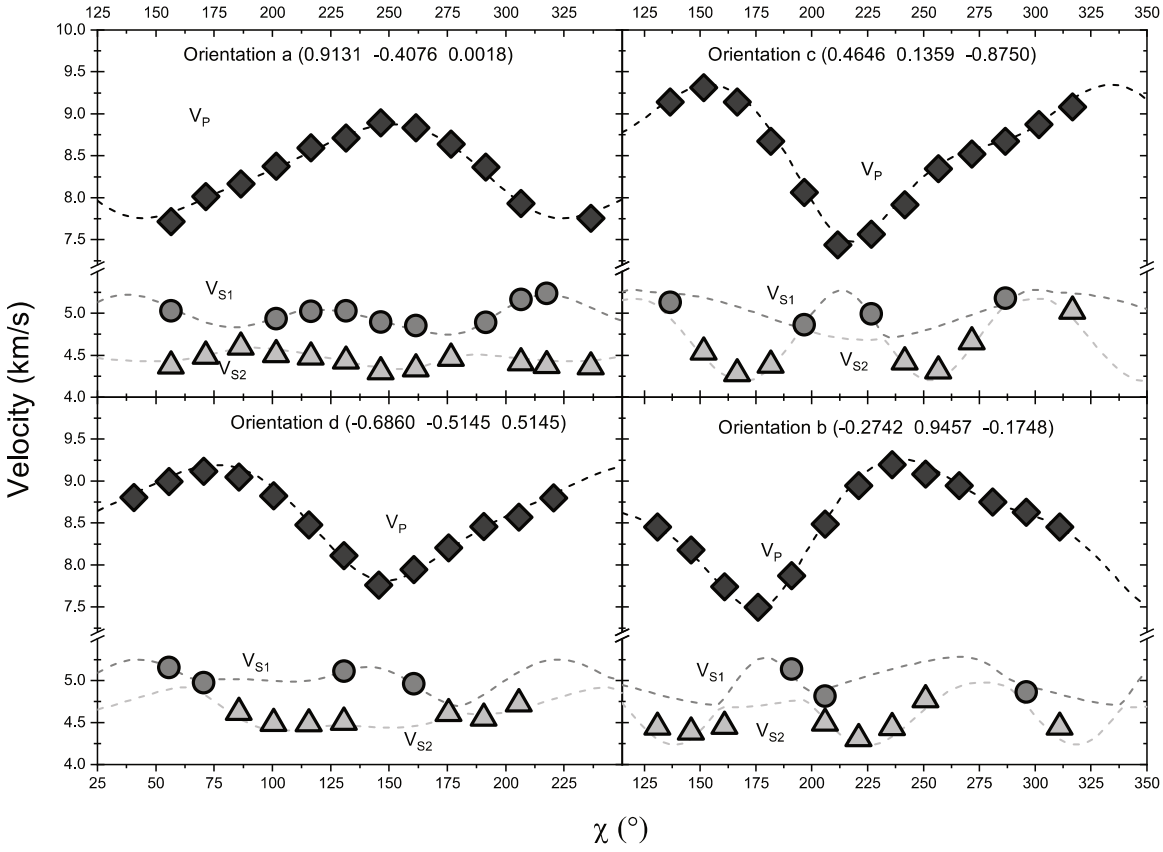

Figure 2. Acoustic velocities measured versus laboratory χ angles for the four orientations of SBB-46. Diamonds, circles, and triangles represent experimentally determined V_p, V_{s1}, and V_{s2}, respectively. The dashed lines were calculated from the best fit single-crystal C_{ij} model. Errors were smaller than the symbols.

The single-crystal elastic properties of anhydrous omphacite at ambient conditions had been measured [39–44] and systematically analyzed within a wide compositional range [44]. As shown in Figure 3, within the Di–Jd solid solution, most elastic moduli showed a close-to-ideal linear mixing trend except C_{13} and C_{23}. The C_{33}, C_{55}, and C_{35} presented in Ref. [44] lay outside the trends determined from other measurements, which can be explained by the high Tschermak content of the sample (12 mol%). The bulk and shear elastic moduli (K_s and G), as well as most of the single-crystal C_{ij}s of the hydrous omphacite SBB-46, were well within the 95% confidence interval determined by all of the previous measurements of anhydrous omphacite samples within the Di–Jd solid solution (Table 1). A few single-crystal elastic moduli such as C_{13}, C_{25}, C_{44}, and C_{66} showed a small decrease within the Di–Jd solid solution (up to ~9 GPa), deviating outside of the 95% confidence interval, which might have been caused by the incorporation of water into its crystal structure (Table 1). However, the decrease of these single-crystal elastic moduli caused by hydration is unlikely to produce a strong seismic anomaly. For example, the ~7% decrease of C_{44} and C_{66} caused by ~710 ppm water transforms to about 3.5% reduction in [010] polarized Vs propagating along the [001] and [100] directions, respectively. Considering the 50–70 vol% of omphacite in the eclogite rock, as well as the elastically isotropic nature of the garnet, it is difficult for the decrease of V_s in the eclogite rock in a realistic scenario to exceed 1%, unless near-perfect alignment of the omphacite crystals takes place in the form of SL-type fabrics [45–48]. In addition, the aggregate V_p and V_s did not show any structural water-induced softening either (Figure 4). Therefore, it is unlikely that the hydration of omphacite crystals would affect the seismic properties of the subducted slab crust.

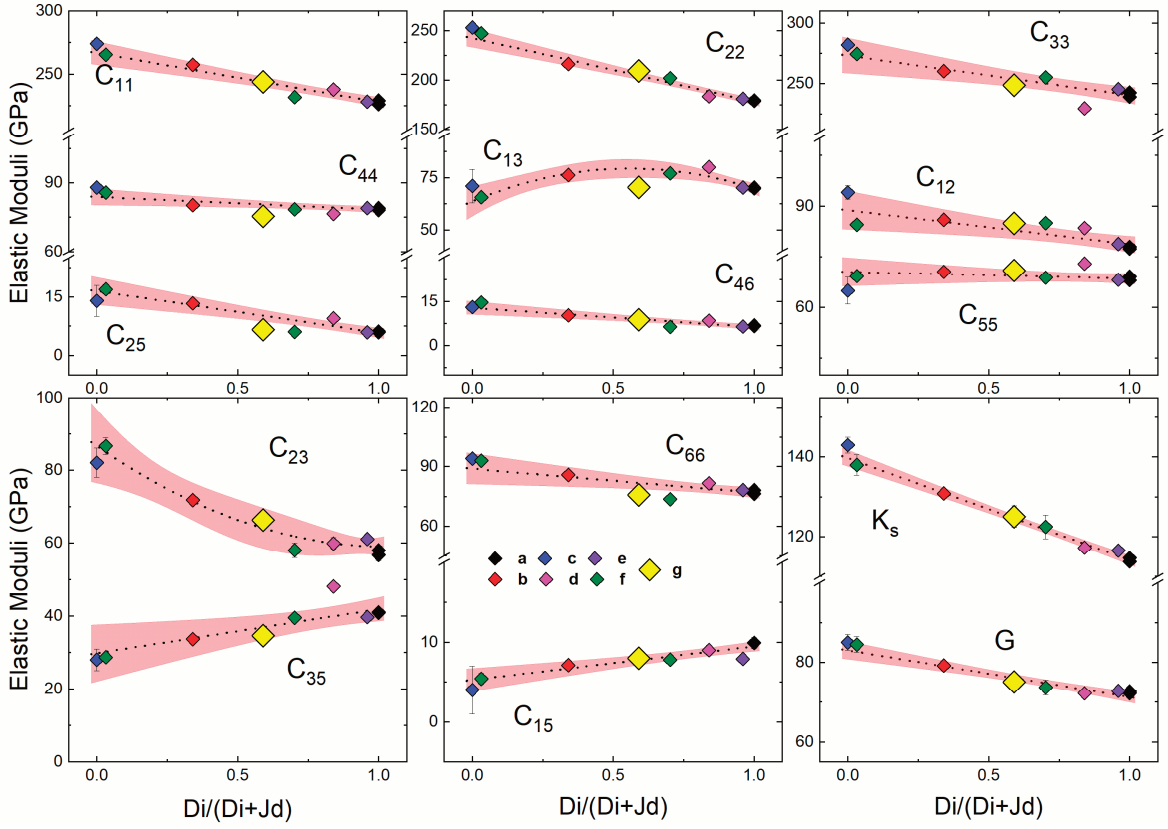

Figure 3. Single-crystal elastic properties of SBB-46 compared with previous studies on anhydrous omphacites within the Di–Jd solid solution as measured by (**a**) Sang et al., 2011 [39], (**b**) Bhagat et al., [40], (**c**) Kandelin and Weidener, 1988 [41], (**d**) Collins and Brown, 1998 [42], (**e**) Isaak and Ohno, 2003 [43], (**f**) Hao et al., 2019 [44]. The results are compared with the hydrous omphacite measured in (**g**) this study. Dashed lines show the compositional dependence of C_{ij}s, K_s, and G. Shaded regions represent the 95% confidence intervals determined in [44].

Table 1. Elastic moduli of the hydrous omphacite sample measured in this study and the anhydrous omphacite with the same chemical composition predicted from Hao et al., 2019 [44]. The uncertainties for the anhydrous omphacite are defined by the 95% confidence intervals shown in Figure 3.

Elastic Moduli	Anhydrous Di59.1Jd40.9	SBB-46 Di59.1Jd40.9 ~710 ppm Water
C_{11} (GPa)	244(4)	245(1)
C_{22} (GPa)	205(4)	210(2)
C_{33} (GPa)	254(6)	249.6(9)
C_{44} (GPa)	81(2)	75.7(9)
C_{55} (GPa)	69(2)	71.2(5)
C_{66} (GPa)	82(2)	76(1)
C_{12} (GPa)	83(2)	85(2)
C_{13} (GPa)	79(4)	70(1)
C_{23} (GPa)	64(6)	66(2)
C_{15} (GPa)	7.7(6)	8.0(6)
C_{25} (GPa)	10(2)	6(1)
C_{35} (GPa)	37(3)	34.7(6)
C_{46} (GPa)	9(1)	8.7(7)
Ks (GPa)	125(1)	125(3)
G (GPa)	76(1)	75(2)

We also calculated three elastic anisotropy indices for the hydrous omphacite SBB-46 and plotted the data along with other anhydrous omphacite samples in the Di–Jd solid solution (Figure 4): (1) The

Universal Anisotropy Index (A^U) which described the overall elastic anisotropy for any materials with arbitrary symmetry, (2) V_p azimuthal anisotropy Index (A^{Vp}) which was the maximum difference in V_p along all crystallographic directions divided by the aggregate V_p, and (3) the polarization anisotropy Index for V_s (D^{Vs}) which measured the maximum velocity difference between two orthogonally polarized V_s that propagated in the same direction. Among these indices, only the A^U for SBB-46 was slightly lower than the expected value for its anhydrous counterpart. This again suggested that the effect of ~710 ppm water on the aggregate elastic properties of omphacite was very small if not negligible. It was also worth noting that Ref. [44] again lay outside the trends determined from all of the other studies probably due to the high Tschermak content (12 mol%) of the sample. This observation is also important for the recent development of elastic geobarometry [26,27]. The elastic anisotropy seems to be a major factor that needs to be taken into account for calculating the *P*s for various geological processes, in particular when the rock has experienced high-grade metamorphism and eclogite facies are found [49–51].

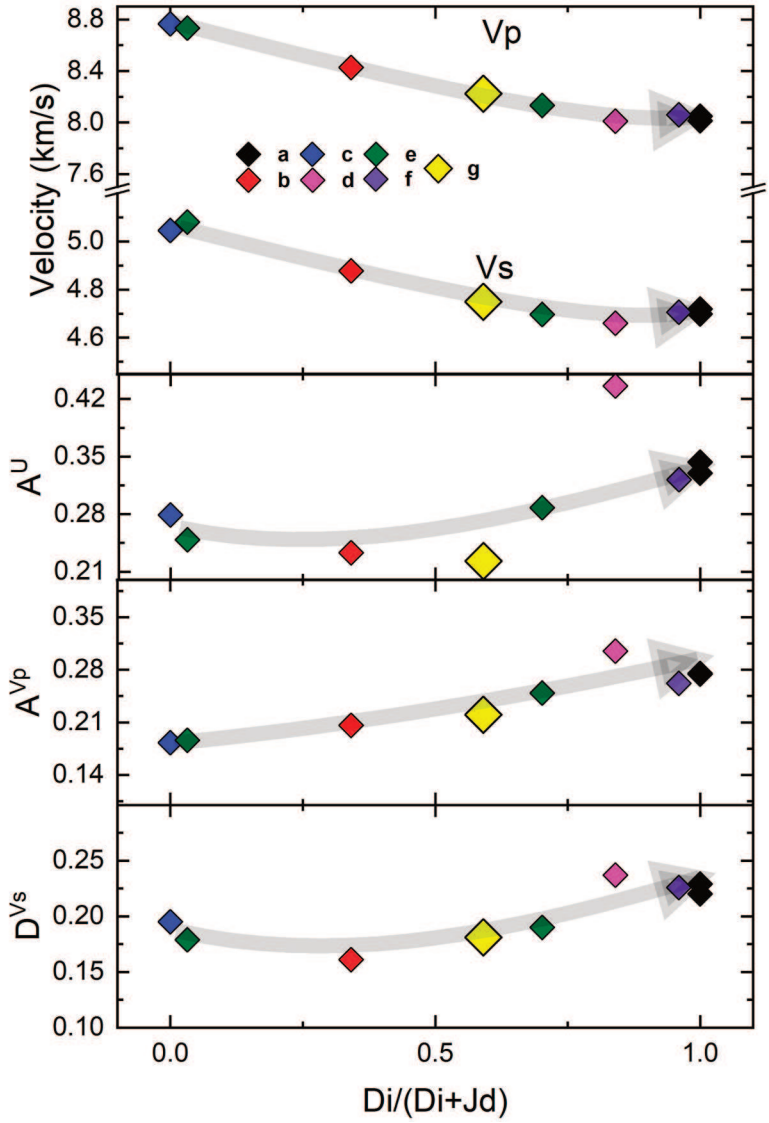

Figure 4. The V_p and V_s, A^U, A^{Vp}, and D^{Vs} of SBB-46 compared with previous studies on anhydrous omphacites (adapted from Hao et al., 2019 [44]) within the Di–Jd solid solution as measured by (**a**) Sang et al., 2011 [39], (**b**) Bhagat et al., [40], (**c**) Kandelin and Weidener, 1988 [41], (**d**) Collins and Brown, 1998 [42], (**e**) Isaak and Ohno, 2003 [43], (**f**) Hao et al., 2019 [44], and (**g**) this study.

4. Conclusions

For the first time, we have experimentally explored the effect of structural water on the single-crystal elastic properties of a hydrous omphacite sample SBB-46. Most of the single-crystal elastic moduli of the hydrous omphacite SBB-46 were well within the 95% confidence interval determined by all the previous measurements of anhydrous omphacite samples within the Di–Jd solid solution. The small decrease of the shear elastic moduli C_{13}, C_{25}, C_{44}, and C_{66} is unlikely to result in a strong seismic anomaly unless the eclogite has experienced extremely high strain and a near-perfect alignment of most omphacite crystals takes place. Based on this study, low to moderate amounts of structural water (~710 ppm) are unlikely to have significant impact on the seismic velocities of the subducted oceanic crust. Further studies of hydrous omphacite at a much higher water concentration (e.g., 1800 ppm [13]) and at high *P*–*T* conditions might provide additional insights.

Author Contributions: Conceptualization, J.S.Z. and W.M.; methodology, J.S.Z., J.R.S., G.J.F., P.D., D.Z.; software, J.S.Z.; validation, J.S.Z. and M.H.; formal analysis, W.M., M.H., J.R.S., G.J.F., P.D.; resources, J.S.Z., J.R.S., G.J.F., P.D., D.Z.; data curation, W.M., J.S.Z., G.J.F., P.D., D.Z.; writing—original draft preparation, W.M.; writing—review and editing, J.S.Z. and everybody else; visualization, W.M., J.S.Z., and M.H.; supervision, J.S.Z.; project administration, J.S.Z.; funding acquisition, J.S.Z.

Funding: This research was funded by National Science Foundation, grant number EAR 1646527 (J.S.Z.). The high-P laser lab was funded by the startup (J.S.Z) at University of New Mexico and National Science Foundation, grant number EAR 1646527 (J.S.Z.). P.D. was supported by the National Science Foundation grant number EAR 1722969. Portions of the X-ray diffraction work were conducted using the X-ray Atlas instrument at the University of Hawaii, funded by NSF grant EAR 1541516. Beamline 13BMC is supported by COMPRES, the Consortium for Materials Properties Research in Earth Sciences under NSF Cooperative Agreement EAR 1661511, and GSECARS funded by NSF (EAR-1634415), and Department of Energy (DOE)—GeoSciences (DE-FG02-94ER14466). This research used resources of the APS, a U.S. DOE Office of Science User Facility operated for the DOE Office of Science by Argonne National Laboratory under contract DE-AC02-06CH11357.

Acknowledgments: The authors thank Zhiyuan Ren and Wenyi Zhou for the help with the experiments.

Conflicts of Interest: The authors declare no conflict of interest. The funders had no role in the design of the study; in the collection, analyses, or interpretation of data; in the writing of the manuscript, or in the decision to publish the results.

References

1. Jacobsen, S.D. Effect of Water on the Equation of State of Nominally Anhydrous Minerals. In *Water in Nominally Anhydrous Minerals*; Walter de Gruyter GmbH: Berlin, Germany, 2018; pp. 321–342. [CrossRef]
2. Liu, L.; Du, J.; Zhao, J.; Liu, H.; Gao, H.; Chen, Y. Elastic Properties of Hydrous Forsterites under High Pressure: First-Principle Calculations. *Phys. Earth Planet. Inter.* **2009**, *176*, 89–97. [CrossRef]
3. Karato, S.I. Mapping Water Content in the Upper Mantle. In *Geophysical Monograph Series*; Blackwell Publishing Ltd.: Hoboken, NJ, USA, 2004; Volume 138, pp. 135–152. [CrossRef]
4. Thompson, A.B. Water in the Earth's Upper Mantle. *Nature* **1992**, *358*, 295–302. [CrossRef]
5. Katayama, I.; Nakashima, S.; Yurimoto, H. Water Content in Natural Eclogite and Implication for Water Transport into the Deep Upper Mantle. *Lithos* **2006**, *86*, 245–259. [CrossRef]
6. Ohtani, E.; Litasov, K.; Hosoya, T.; Kubo, T.; Kondo, T. Water Transport into the Deep Mantle and Formation of a Hydrous Transition Zone. *Phys. Earth Planet. Inter.* **2004**, *143*, 255–269. [CrossRef]
7. Skogby, H. Water in Natural Mantle Minerals I: Pyroxenes. *Rev. Mineral. Geochem.* **2006**, *62*, 155–167. [CrossRef]
8. Xia, Q.K.; Liu, J.; Kovács, I.; Hao, Y.T.; Li, P.; Yang, X.Z.; Chen, H.; Sheng, Y.M. Water in the Upper Mantle and Deep Crust of Eastern China: Concentration, Distribution and Implications. *Natl. Sci. Rev.* **2019**, *6*, 125–144. [CrossRef]
9. Rapp, R.P.; Irifune, T.; Shimizu, N.; Nishiyama, N.; Norman, M.D.; Inoue, T. Subduction Recycling of Continental Sediments and the Origin of Geochemically Enriched Reservoirs in the Deep Mantle. *Earth Planet. Sci. Lett.* **2008**, *271*, 14–23. [CrossRef]
10. Liu, L.; Zhang, J.S. Differential Contraction of Subducted Lithosphere Layers Generates Deep Earthquakes. *Earth Planet. Sci. Lett.* **2015**, *421*, 98–106. [CrossRef]

11. Irifune, T.; Sekine, T.; Ringwood, A.E.; Hibberson, W.O. The Eclogite–Garnetite Transformations at High Pressure and Some Geophysical Implications.Pdf. *Earth Planet. Sci. Lett.* **1986**, *77*, 245–256. [CrossRef]
12. Gavrilenko, P. Water Solubility in Diopside. Ph.D. Thesis, Bayerisches Geoinstitut, University Bayreuth, Bayreuth, Germany, 2008; p. 139.
13. Smyth, J.R.; Bell, D.R.; Rossman, G.R. Incorporation of hydroxyl in upper-mantle clinopyroxenes. *Nature* **1991**, *351*, 732–735. [CrossRef]
14. Wen, S.; Zhendong, Y.; Bolin, C.; Kai, Y. Role of Water in Deformed Omphacite in UHP Eclogite from the Dabie Mountains, Eastern China. *Acta Geol. Sin. Engl. Ed.* **2003**, *77*, 320–325. [CrossRef]
15. Weis, F.A.; Ros, L.; Reichart, P.; Skogby, H.; Kristiansson, P.; Dollinger, G. Hydrogen Concentration Analysis in Clinopyroxene Using Proton–Proton Scattering Analysis. *Phys. Chem. Miner.* **2018**, *45*, 669–678. [CrossRef]
16. Weis, F.A.; Skogby, H.; Troll, V.R.; Deegan, F.M.; Dahren, B. Magmatic Water Contents Determined through Clinopyroxene: Examples from the Western Canary Islands, Spain. *Geochem. Geophys. Geosys.* **2015**, *16*, 2127–2146. [CrossRef]
17. Warren, J.M.; Hauri, E.H. Pyroxenes as Tracers of Mantle Water Variations. *J. Geophys. Res. Solid Earth* **2014**, *119*, 1851–1881. [CrossRef]
18. Bromiley, G.D.; Keppler, H. An Experimental Investigation of Hydroxyl Solubility in Jadeite and Na-Rich Clinopyroxenes. *Contrib. Mineral. Petrol.* **2004**, *147*, 189–200. [CrossRef]
19. Ghosh, S.; Ohtani, E.; Litasov, K.D.; Suzuki, A.; Dobson, D.; Funakoshi, K. Effect of Water in Depleted Mantle on Post-Spinel Transition and Implication for 660 km Seismic Discontinuity. *Earth Planet. Sci. Lett.* **2013**, *371–372*, 103–111. [CrossRef]
20. Ghosh, S.; Ohtani, E.; Litasov, K.D.; Suzuki, A.; Dobson, D.; Funakoshi, K. Corrigendum to "Effect of Water in Depleted Mantle on Post-Spinel Transition and Implication for 660 Km Seismic Discontinuity" [Earth Planet. Sci. Lett. 371–372 (2013) 103–111]. *Earth Planet. Sci. Lett.* **2013**, *382*, 85–86. [CrossRef]
21. Jacobsen, S.D.; Jiang, F.; Mao, Z.; Duffy, T.S.; Smyth, J.R.; Holl, C.M.; Frost, D.J. Effects of Hydration on the Elastic Properties of Olivine. *Geophys. Res. Lett.* **2008**, *35*. [CrossRef]
22. Mao, Z.; Jacobsen, S.D.; Jiang, F.; Smyth, J.R.; Holl, C.M.; Duffy, T.S. Elasticity of Hydrous Wadsleyite to 12 GPa: Implications for Earth's Transition Zone. *Geophys. Res. Lett.* **2008**, *35*. [CrossRef]
23. Mao, Z.; Lin, J.F.; Jacobsen, S.D.; Duffy, T.S.; Chang, Y.Y.; Smyth, J.R.; Frost, D.J.; Hauri, E.H.; Prakapenka, V.B. Sound Velocities of Hydrous Ringwoodite to 16GPa and 673K. *Earth Planet. Sci. Lett.* **2012**, *331–332*, 112–119. [CrossRef]
24. Wang, W.; Walter, M.J.; Peng, Y.; Redfern, S.; Wu, Z. Constraining Olivine Abundance and Water Content of the Mantle at the 410-Km Discontinuity from the Elasticity of Olivine and Wadsleyite. *Earth Planet. Sci. Lett.* **2019**, *519*, 1–11. [CrossRef]
25. Xu, J.; Zhang, D.; Fan, D.; Zhang, J.S.; Hu, Y.; Guo, X.; Dera, P.; Zhou, W. Phase Transitions in Orthoenstatite and Subduction Zone Dynamics: Effects of Water and Transition Metal Ions. *J. Geophys. Res. Solid Earth* **2018**, *123*, 2723–2737. [CrossRef]
26. Angel, R.J.; Nimis, P.; Mazzucchelli, M.L.; Alvaro, M.; Nestola, F. How Large Are Departures from Lithostatic Pressure? Constraints from Host–Inclusion Elasticity. *J. Metamorph. Geol.* **2015**, *33*, 801–813. [CrossRef]
27. Angel, R.J.; Mazzucchelli, M.L.; Alvaro, M.; Nestola, F. EosFit-Pinc: A Simple GUI for Host-Inclusion Elastic Thermobarometry. *Am. Mineral.* **2019**, *102*, 1957–1960. [CrossRef]
28. Maxisch, T.; Ceder, G. Elastic Properties of Olivine Lix FePO4 from First Principles. *Phys. Rev. B-Condens. Matter Mater. Phys.* **2006**, *73*, 174112. [CrossRef]
29. Sinogeikin, S.V.; Katsura, T.; Bass, J.D. Sound Velocities and Elastic Properties of Fe-Bearing Wadsleyite and Ringwoodite. *J. Geophys. Res. Solid Earth* **1998**, *103*, 20819–20825. [CrossRef]
30. Inoue, T.; Weidner, D.J.; Northrup, P.A.; Parise, J.B. Elastic Properties of Hydrous Ringwoodite (γ-Phase) in Mg_2SiO_4. *Earth Planet. Sci. Lett.* **1998**, *160*, 107–113. [CrossRef]
31. Zhang, D.; Dera, P.K.; Eng, P.J.; Stubbs, J.E.; Zhang, J.S.; Prakapenka, V.B.; Rivers, M.L. High Pressure Single Crystal Diffraction at PX^2. *J. Vis. Exp.* **2017**, *119*, e54660. [CrossRef]
32. Prescher, C.; Prakapenka, V.B. DIOPTAS: A Program for Reduction of Two-Dimensional X-Ray Diffraction Data and Data Exploration. *High Press. Res.* **2015**, *35*, 223–230. [CrossRef]
33. Zhang, J.S.; Bass, J.D.; Taniguchi, T.; Goncharov, A.F.; Chang, Y.Y.; Jacobsen, S.D. Elasticity of Cubic Boron Nitride under Ambient Conditions. *J. Appl. Phys.* **2011**, *109*, 063521. [CrossRef]

34. Zhang, J.S.; Bass, J.D.; Zhu, G. Single-Crystal Brillouin Spectroscopy with CO_2 Laser Heating and Variable Q. *Rev. Sci. Instrum.* **2015**, *86*, 063905. [CrossRef] [PubMed]
35. Oberti, R.; Caporuscio, F.A. Crystal chemistry of clinopyroxenes from mantle eclogites: A study of the key role of the M2 site population by means of crystal-structure refinement. *Am. Mineral.* **1991**, *76*, 1141–1152.
36. Fleet, M.E.; Henznrnc, C.T.; Bancroft, G.M.; Aldridge, L.P. Omphacite Studies, I. The P2ln-C2 /c Transformation. *Am. Mineral.* **1978**, *63*, 1100–1106.
37. Hao, M.; Zhang, J.S.; Pierotti, C.E.; Ren, Z.; Zhang, D. High-Pressure Single-Crystal Elasticity and Thermal Equation of State of Omphacite and Their Implications for the Seismic Properties of Eclogite in the Earth's Interior. *J. Geophys. Res. Solid Earth* **2019**, *124*, 2368–2377. [CrossRef]
38. Hill, R. Elastic Properties of Reinforced Solids: Some Theoretical Principles. *J. Mech. Phys. Solids* **1963**, *5*, 357–372. [CrossRef]
39. Sang, L.; Vanpeteghem, C.B.; Sinogeikin, S.V.; Bass, J.D. The Elastic Properties of Diopside, $CaMgSi_2O_6$. *Am. Mineral.* **2011**, *96*, 224–227. [CrossRef]
40. Bhagat, S.S.; Bass, J.D.; Smyth, J.R. Single-Crystal Elastic Properties of Omphacite-C2/c by Brillouin Spectroscopy. *J. Geophys. Res.* **1992**, *97*, 6843–6848. [CrossRef]
41. Kandelin, J.; Weidener, D.J. The single-crystal elastic properties of jadeite. *Phys. Earth Planet. Inter.* **1988**, *3*, 251–260. [CrossRef]
42. Brown, J.M.; Collins, M.D. Elasticity of an Upper Mantle Clinopyroxene. *Phys. Chem. Miner.* **1998**, *26*, 7–13. [CrossRef]
43. Isaak, D.G.; Ohno, I. Elastic Constants of Chrome-Diopside: Application of Resonant Ultrasound Spectroscopy to Monoclinic Single-Crystals. *Phys. Chem. Miner.* **2003**, *30*, 430–439. [CrossRef]
44. Hao, M.; Pierotti, C.E.; Tkachev, S.; Prakapenka, V.; Zhang, J.S. The Single-Crystal Elastic Properties of the Jadeite-Diopside Solid Solution and Their Implications for the Composition-Dependent Seismic Properties of Eclogite. *Am. Mineral.* **2019**, *104*, 1016–1021. [CrossRef]
45. Bascou, J.; Barruol, G.; Vauchez, A.; Mainprice, D.; Egydio-Silva, M. EBSD-Measured Lattice-Preferred Orientations and Seismic Properties of Eclogites. *Tectonophysics* **2001**, *342*, 61–80. [CrossRef]
46. Bascou, J.; Tommasi, A.; Mainprice, D. Plastic Deformation and Development of Clinopyroxene Lattice Preferred Orientations in Eclogites. *J. Struct. Geol.* **2002**, *24*, 1357–1368. [CrossRef]
47. Ulrich, S.; Mainprice, D. Does Cation Ordering in Omphacite Influence Development of Lattice-Preferred Orientation? *J. Struct. Geol.* **2005**, *27*, 419–431. [CrossRef]
48. Zhang, J.; Green, H.W.; Bozhilov, K.N. Rheology of Omphacite at High Temperature and Pressure and Significance of Its Lattice Preferred Orientations. *Earth Planet. Sci. Lett.* **2006**, *246*, 432–443. [CrossRef]
49. Mazzucchelli, M.L.; Reali, A.; Morganti, S.; Angel, R.J.; Alvaro, M. Elastic Geobarometry for Anisotropic Inclusions in Cubic Hosts. *Lithos* **2019**, *350–351*, 105218. [CrossRef]
50. Alvaro, M.; Mazzucchelli, M.L.; Angel, R.J.; Murri, M.; Campomenosi, N.; Scambelluri, M.; Nestola, F.; Korsakov, A.; Tomilenko, A.A.; Marone, F.; et al. Fossil Subduction Recorded by Quartz from the Coesite Stability Field. *Geology* **2020**, *48*, G46617.1. [CrossRef]
51. Bonazzi, M.; Tumiati, S.; Thomas, J.B.; Angel, R.J.; Alvaro, M. Assessment of the Reliability of Elastic Geobarometry with Quartz Inclusions. *Lithos* **2019**, *350–351*, 105201. [CrossRef]